Mass Spectrometry & Purification Techniques

Monte et al., Mass Spectrom Purif Tech 2016, 2:1
DOI: 10.4172/2469-9861.1000112

Research Article Open Access

Tobacco Smoke-Induced Alterations in Hepatic Lipid Profiles Demonstrated by Imaging Mass Spectrometry

Suzanne M de la Monte[2,4]*, Ming Tong[2], Kavin Nunez[1], Emine Yalcin[2], Jared Kay[1], Amit R Agarwal[3] and Enrique Cadenas[3]

[1]*Molecular Pharmacology, Physiology and Biotechnology Graduate Program, Brown University, Providence, RI, USA*
[2]*Liver Research Center, Department of Medicine, Rhode Island Hospital and the Alpert Medical School of Brown University, Providence, RI, USA*
[3]*Department of Pharmacology and Pharmaceutical Sciences, School of Pharmacy, University of Southern California, Los Angeles, CA, USA*
[4]*Division of Neuropathology and Department of Pathology, Neurology and Neurosurgery, Rhode Island Hospital and the Alpert Medical School of Brown University, Providence, RI, USA*

Abstract

To account for differences in susceptibility to alcoholic liver disease (ALD), tobacco smoking should be evaluated as a potential cofactor given the very high percentage of heavy drinkers also smoke, and the NNK tobacco-specific nitrosamine was shown to cause steatohepatitis and exacerbate molecular and biochemical effects of alcohol on the liver. Since one of the key factors linked to ALD progression is dysregulated lipid metabolism, we examined effects of cigarette smoke (CS) exposures on hepatic lipid profiles using matrix-assisted laser desorption and ionization imaging mass spectrometry (MALDI-IMS). Adult male A/J mice were exposed to air (8 weeks; A8), CS for 4 (CS4) or 8 (CS8) weeks; or CS8 with 2 weeks recovery (CS8+R). MALDI-IMS demonstrated broad CS-associated reductions in hepatic phospholipids that were partly ameliorated by short-term recovery. Principal component analysis revealed CS-associated shifts in phospholipid profiles that also partly normalized with recovery. Heatmaps demonstrated striking effects of CS with graded responses to exposure duration and recovery. Importantly, several of the CS-induced lipid profile alterations persisted after air recovery, suggesting that the responses had become permanent, whereas others worsened with CS exposure duration and were either sustained or revered with recovery.

Keywords: Tobacco; Cigarette smoke; Mouse model; Phospholipids; Mass spectrometry; MALDI imaging

Introduction

Alcohol abuse is a leading cause of liver related morbidity and mortality [1-3] due to progression of steatohepatitis to escalating chronic disease states that culminate in cirrhosis and eventually liver failure [4-6]. In alcoholic liver disease (ALD), hepatic function deteriorates due to adverse interactive effects of insulin resistance [7-9], cytotoxic and lipotoxic injury [10-13], inflammation [10,14], oxidative and ER stress [15-18], metabolic and mitochondrial dysfunction [5,19], decreased DNA synthesis [8,20], and increased cell death [11].

Since progressive ALD occurs in only a percentage of individuals who regularly consume alcohol, increased understanding of its pathogenesis, including the role of co-factors, could help improve preventive, diagnostic and therapeutic approaches. In this regard, it is noteworthy that a very high percentage (~80%) of heavy drinkers/alcoholics also abuse tobacco products, typically by cigarette smoking [21,22], yet little is known about non-carcinogenic, degenerative effects of smoking, apart from cardiovascular and pulmonary diseases. Nonetheless, the potential role of tobacco smoke as a cofactor in ALD was suggested by the findings that: 1) chronic low level exposures to 4-(methylnitrosamino)-1-(3-pyridyl)-1-butanone or nicotine-derived nitrosamine ketone (NNK), one of the most abundant nitrosamines present in tobacco smoke [23-26], cause steatohepatitis with insulin resistance, along with most other abnormalities present in ALD [27]; 2) chronic exposures to ethanol and NNK caused striking and partially overlapping alterations in hepatic lipid profiles as demonstrated by matrix-assisted laser desorption and ionization-imaging mass spectrometry (MALDI-IMS) [28]; and 3) both ethanol and NNK cause hepatic insulin resistance with impaired signaling through PI3K-Akt pathways, DNA damage, lipid peroxidation, pro-inflammatory cytokine activation, and ceramide accumulation, and dual exposures worsened the severity of steatohepatitis and associated molecular and biochemical abnormalities compared with either exposure alone [27].

The present work directly examines the effects of cigarette smoke (CS) exposures on liver function, using MALDI-IMS to focus on alterations in hepatic lipid profiles. This approach was taken to assess the degree to which CS exposures cause metabolic dysfunction, and whether the abnormalities could be reversed by short-term smoking cessation.

Methods

Experimental model

These studies utilized an A/J mouse model similar to the one developed in 2002 [29]. The A/J strain was used because of its high susceptibility to lung defects after tobacco smoke exposure [30]. Furthermore, the A/J model replicates the human experience in that following chronic (5 months) tobacco smoke exposure, plasma cotinine levels are comparable to those in active human smokers, and the mice develop emphysema and lung tumors [29,31]. However, the relatively short-term exposures that we employed do not produce these end-point diseases [31-33].

Adult (8 weeks old) A/J male mice (N=5-6/group) were exposed to cigarette smoke (CS) or air as follows: 1) 8 weeks of room air only (A8); 2) 4 weeks CS (CS4); 3) CS8; 4) CS8 followed by 2 weeks recovery (CS8+R) [32,33]. CS was generated from research grade Kentucky 3R4F cigarettes (Tobacco Research Institute, University of Kentucky, Lexington, KY) using an industry standard Teague Enterprises, TE-10 Smoking Machine (Davis, CA). The cigarettes contained 11 mg of total particulate matter (TPM) and 0.73 mg of nicotine. Side-stream

***Corresponding author:** Suzanne M. de la Monte, MD, MPH, Pierre Galletti Research Building, Rhode Island Hospital, 55 Claverick Street, Room 419, Providence, Rhode Island, United States of America, Tel: 401-444-7364; Fax: 401-444-2939; E-mail: Suzanne_DeLaMonte_MD@Brown.edu

Received March 17, 2016; **Accepted** March 29, 2016; **Published** December 04, 2016

Citation: Monte SML, Tong M, Nunez K, Yalcin E, Kay J, et al. (2016) Tobacco Smoke-Induced Alterations in Hepatic Lipid Profiles Demonstrated by Imaging Mass Spectrometry. Mass Spectrom Purif Tech 2: 112. doi:10.4172/2469-9861.1000112

and mainstream smoke were mixed in a ratio of 89% to 11%, which is similar to environmental tobacco smoke exposures. Six cigarettes were puffed simultaneously, one time per minute for 9 puffs. The cigarettes were burned for 6 hours/day, 5 days/week and for 4 or 8 weeks duration. Mice were adapted to CS by ramping up concentration and exposure period in the first week.

The chamber atmosphere was monitored for total suspended particles. The smoke exposure system involved burning of cigarettes in one location, and then delivering the smoke to exposure chambers that housed the mice. In the vicinity where cigarettes were burned, the CO levels reached 24 ppm, which is well above natural air (less than 0.5 ppm) but comparable to the amounts present in tobacco smoke exhaled by humans (25-30 ppm) [34]. The atmosphere within the mouse CS exposure chambers had 21% oxygen and approximately 3 ppm of CO. Before use, the cigarettes were kept for 48 h in a standardized atmosphere humidified with 70% glycerol-30% water. Throughout the experiment, mice were housed under humane conditions and kept on a 12-hour light/dark cycle with free access to food. All experiments were performed in accordance with protocols approved by the University of Southern California's Institutional Animal Care and Use Committee, and conformed to guidelines established by the National Institutes of Health.

Liver tissue collection and lipid extraction

Freshly harvested liver tissue was snap frozen and stored at -80°C for biochemical studies. Lipids were extracted from fresh frozen tissue with 2:1 chloroform-methanol [35].

Sample preparation for Matrix-Assisted Laser Desorption/ Ionization Imaging Mass Spectrometry (MALDI-IMS)

Fresh frozen tissue (3-5 mm diameter) samples were equilibrated to -20°C and mounted onto cryostat chucks using the minimum amount of Optimal Cutting Temperature Compound (OCT; Tissue-Tek®; Sakura Finetek, Torrance, CA, USA) that avoided contamination of the slide. Frozen sections (10 µm thick) were thaw-mounted onto indium tin oxide (ITO)-coated slides (Delta Technologies, Loveland, CO) and vacuum dried for 2 hours in a desiccator. After washing with HPLC grade ammonium formate (50 mM, pH 6.4) to remove salts and enhance lipid analysis [36], the slides were re-dried and sublimed with 2,5-dehydroxybenzoic acid (DHB; Sigma-Aldrich Co, St. Louis, MO) [37] as the matrix [38].

MALDI-IMS/Time of Flight and Data Analysis for Lipid Ions

Imaging was performed with a reflectron geometry MALDI-TOF/TOF mass spectrometer (Ultraflextreme, Bruker Daltonics, Bremen, Germany). Analyses were performed by focusing a Smartbeam II Nd:YAG laser onto a ~100 µm area, and Imaging data were acquired in the negative ion mode at a lateral resolution of 100 µm, summing 500 shots/array position at a laser repetition rate of 1000 Hz. Data were processed using FlexAnalysis v3.4 and visualized with FlexImaging software v4.0. Results were normalized to total ion count, which prevents ion suppression and variation across tissue sections and matrix preparations, and analyzed statistically using ClinProTools v3.0. Post-imaged and adjacent sections fixed in formalin and stained with H&E were used to co-register regions of interest (ROI) with the MALDI-IMS. Lipids were identified by comparing the precursor and product ion m/z values with those catalogued in the LIPID MAPS prediction tool database (http://www.lipidmaps.org/tools/index.html). Their identities were confirmed by tandem mass spectrometry (MS/MS) in the LIFT-TOF/TOF mode.

Heatmap statistics

Heatmaps were constructed using Version 3.2 of R software [39,40]. Exploratory data analysis verified the quality of observed data. The data were imported into R as a comma delimited values table, excluding the control genes (Actin and HPRT). Several transformations were applied to the row values. To scale the data, row means were subtracted from each cell. The resulting values were further divided by the standard deviation in order to obtain a z-score of each individual cell yielding row values with a mean of 0 and S.D. of 1. The resulting values were plotted using a cosmetically modified version of a latent R heatmap function using a 6-color palette. We also applied hierarchical clustering algorithm using Euclidean distance function on the overall table to display a dendrogram of mRNAs.

Results

Matrix-assisted Laser Desorption Ionization-Imaging Mass Spectrometry (MALDI-IMS)

MALDI-IMS approach: MALDI-IMS enables visualization of specific molecules, including drugs, lipids, peptides, and proteins in tissue sections [41,42]. MALDI-IMS is remarkably sensitive and specific as it enables detection of ions with known mass/charge (m/z) characteristics [43,44]. Importantly, MALDI-IMS can be used to examine tissue biochemical abnormalities, complementing histopathological and molecular studies. Hepatic steatosis and steatohepatitis are among the most challenging disease entities in which we lack the ability to decipher pathogenesis and understand the contributions of various exposures to disease. Lipids have great structural diversity [45] yet despite their relative structural simplicity, the cellular lipidome's composition is complex and its functions are diverse. For example, lipids have critical roles in providing structural integrity to membranes; they serve as energy reservoirs (triglycerides); and they are used to generate precursor molecules for second messenger signaling [46].

MALDI-IMS analysis of hepatic lipid profiles: Whole slice images were obtained by MALDI-IMS in the negative ion mode, and adjacent Hematoxylin and Eosin (H&E)-stained sections were used to delineate standardized size and shape regions of interest (ROI) for co-registration with the MALDI images. The Peak Statistic report identified 67 distinct m/z lipid ions (m/z=705.54-1061.87) within the ROIs (Supplementary Table 1). We performed tandem mass spectrometry (MS/MS) using MALDI-LIFT-TOF/TOF (negative ion mode) to identify 15 selected lipid ions directly in liver tissue. Following laser desorption/ionization and time-of-flight m/z detection, the lipid ion fragmentation patterns were analyzed using the LIPID MAPS prediction tool. Thirteen of the lipid ions were identified as phospholipids, i.e., phosphatidylserine (PS), phosphatidylethanolamine (PE), or phosphatidylinositol (PI); however, the remaining two lipid ions could not be assigned due to their low abundances/intensities. The main treatment effects were that 1) CS exposures broadly reduced phospholipid ion intensities relative to control; 2) phospholipid levels were reduced to greater extents in CS4 and CS8+R compared with CS8 livers; and 3) phosphatidylinositols were the dominant phospholipid species altered by CS exposure.

Structural assignment of phospholipids

In the negative ion mode of LIFT-TOF/TOF, phospholipids characteristically lose neutral carboxylic acid (RCOOH) and ketone ($R_2CH=C=O$) from their precursor ions ($[M-H]^-$), and acyl chain assignment is enabled by loss of the neutral fragment and fatty acid anions.

Phosphatidylserine identification: Phosphatidylserines (PS) were identified by loss of the serine group from the negative ion product spectrum, and resultant generation of a characteristic [M-H-serine]$^-$ ion fragment. For example, the most abundant fragment peak in the MS/MS spectrum for PS (38:4) had an m/z of 723.8 corresponding to the [M-H-serine]$^-$ ion (Figure 1A). PS acyl chains were identified by assigning fatty acids based upon 5 criteria, including: 1) neutral loss of the substitution nucleophile 1 (sn1) carboxylic acid and serine from the precursor ion ([M-H]) at m/z 439; 2) neutral loss of the sn2 carboxylic acid and serine from precursor ion at m/z 419; 3) loss of sn1 acyl chain as a ketene (RCH=C=O) and serine from precursor ion at m/z 457 (not shown), 4) loss of sn2 acyl chain as a ketene (RCH=C=O) and serine from precursor ion at m/z 437, and 5) the presence of sn1 carboxyl ion at m/z 283 and sn2 carboxyl ion at m/z 303.

Phosphatidylethanolamine identification: Phosphatidylethanolamines (PE; Figure 1B) have an ethanolamine phosphate head group. The PE (38:4) was identified at m/z 766.8; its ethanolamine ion had an m/z of 140. PE acyl chains were identified by assigning fatty acids based on: 1) neutral loss of the sn2 carboxylic acid at m/z 462; 2) loss of the sn2 acyl chain as a ketene at m/z 480; 3) loss of the sn1 carboxylic acid (m/z 283); and 4) loss of the sn2 carboxylic acid (m/z 303).

Phosphatidylinositol identification: Phosphatidylinositols (PI) have inositol phosphate head group ions within the product ion spectra. Example data corresponding to the product ion spectrum of the m/z 885.7 [M-H] parent ion are depicted in Figure 1C. The inositol phosphate head group ion was identified at m/z 241, and with loss of a water molecule, the m/z was 223. Glycerophosphoinositol, with or without loss of a water molecule was identified at m/z's of 297 and 315. Fragment ions of the fatty acyl chains were identified as follows: 1) m/z's of 283 and 303 represented C18:0 and C20:5 fatty acid anions; 2) m/z products at 439 and 419 corresponded to the precursor ion with neutral loss of the inositol and sn1 or sn2 carboxylic acid; 3) m/z 437 represents precursor ion with loss of the sn2 acyl chain as ketone and inositol; 4) m/z's of 601 and 581 correspond to the precursor ion with neutral loss of the sn1 or sn2 carboxylic acid group; 5) m/z's of 619 and 599 represent precursor ion with loss of sn1 and sn2 acyl chains as ketone; and 6) m/z 723 resulted from loss of inositol from the precursor ion.

CS exposure effects on phospholipid expression

MALDI-IMS analysis demonstrated that CS exposures and durations differentially alter hepatic phosphatidylserine and phosphatidylinositol, but not phosphatidylethanolamine levels (Table 1; Figures 2 and 3). The MALDI images and m/z 766.8 ion peak profiles demonstrate similar hepatic levels of PE(38:4) in all groups (Figures 2A and 3; Table 1).

In contrast, CS4 livers had strikingly reduced levels of m/z's 810.8, 834.8, 857.8, 883.8, and 885.7 corresponding to PS(38:4), PS(40:6), PI(36:4), PI(38:5), and PI(38:4), while CS8 livers had similar or somewhat higher levels of the same phospholipids relative to control (Figures 2B and 3; Table 1). In the CS8+R livers, these phospholipid ion intensities and profiles were intermediate between CS4 and control. Two additional phospholipids with m/z's of 910.8 and 912.9, representing PI(40:5) and PI(40:4) were abundantly expressed in control liver and similarly reduced in CS4, CS8 and CS8+R livers (Figure 2C; Table 1). Similar trends were observed with respect to PI(44:9)-m/z 958.9 and PI(44.8-m/z 960.9 (Table 1). Finally, phosphoinositol ions with m/z's 934.8 (PI(41:0)), 938.9 (PI42:5)), and 962.8 (PI(18:0/25:0)), and not further characterized phospholipid ions with m/z's 932.7 and 947.7 were similarly reduced by CS exposure, irrespective of duration and interval recovery (Table 1).

Tandem mass spectrometry (MS/MS) with MALDI LIFT-TOF/TOF was used to fragment lipids in the negative ion mode and lipid species assignment was achieved by searching the LIPID MAPS database. Abbreviations and codes: m/z=mass/charge; PE=phosphatidylethanolamine; PS=phosphatidylserine; PI=phosphatidylinositol; A8=air exposure for 8 weeks (control); CS=cigarette smoke exposure for 4 weeks; CS8=cigarette smoke exposure for 8 weeks; CS8+R= CS8 followed by 2 weeks recovery; ↑ increased, ↓ decreased, or ↔ unchanged relative to control.

Heatmap analysis

The heatmap generated with hierarchical clustering illustrates overall effects of CS exposures on hepatic lipid ion expression (Figure 4). The dendrogram shows 3 main clusters (a, b, c) and 8 sub-clusters. In the Cluster a, lipid ion expression was lowest in A8. In Sub-Cluster a1, lipid ion levels were either unchanged or increased moderately in CS4, then further increased in CS8. CS8+R resulted in similar or higher lipid ion levels compared with CS8. In Sub-Cluster a2, the general trend was that lipid ion levels gradually increased from A8 to CS4, then CS8 and finally CS8+R. In Cluster b, A8 livers had moderate to high lipid ion levels, whereas CS4 had sharply lower levels. Sub-Cluster b1 was associated with persistently low lipid ion levels in CS8, while b2 showed recovery or elevated lipid ion expression. In both b1 and b2, CS8+R had nearly normalized lipid ion expression relative to A8. In Cluster c, the largest, A8 samples nearly always had the highest lipid ion levels, and CS exposures mainly reduced hepatic lipid ion expression. Sub-Clusters c2a and c2b showed similar or higher lipid ion levels in CS4 relative to A8, sharply reduced expression in the CS8 group, and either partial recovery (c2a) or sustained inhibition (c2b) in CS8+R. Sub-Cluster c2c was characterized by sustained inhibition of lipid ion expression with CS exposures, while c2d was associated with progressive declines in lipid ion expression from A8 to CS4 followed by CS8. Within c2d, low lipid ion expression was either sustained further reduced in CS8+R relative to CS8. In essence, CS exposures had clear effects on the broad array of lipid expressed in liver. Some lipid ions were increased but

m/z	Lipid assignment	CS4	CS8	CS8+R
766.8	PE(38:4)	↔	↔	↔
810.8	PS(38:4)	↓	↔	↓
834.8	PS(40:6)	↓	↔	↓
857.8	PI(36:4)	↓	↔	↓
883.8	PI(38:5)	↓	↔	↓
885.7	PI(38:4)	↓	↔	↓
910.8	PI(40:5)	↓↓	↓	↓↓
912.9	PI(40:4)	↓↓	↓	↓↓
932.7	ND	↓↓	↓	↓↓
934.8	PI(41:0)	↓	↓	↓
938.9	PI(42:5)	↓	↓	↓
947.7	ND	↓	↓	↓
958.9	PI(44:9)	↓↓	↓	↓↓
960.9	PI(44:8)	↓↓	↓	↓↓
962.8	PI(43:0)	↓	↓	↓

Table 1: Lipid assignments by tandem mass spectrometry. Tandem mass spectrometry (MS/MS) with MALDI LIFT-TOF/TOF was used to fragment lipids in the negative ion mode and lipid species assignment was achieved by searching the LIPID MAPS database. Abbreviations and codes: m/z=mass/charge; PE=phosphatidylethanolamine; PS=phosphatidylserine; PI=phosphatidylinositol; CS=cigarette smoke exposure for 4 weeks; CS8=cigarette smoke exposure for 8 weeks; CS8+R=CS8 followed by 2 weeks recovery; ↓ decreased, ↓↓ sharply decreased, or ↔ unchanged relative to control.

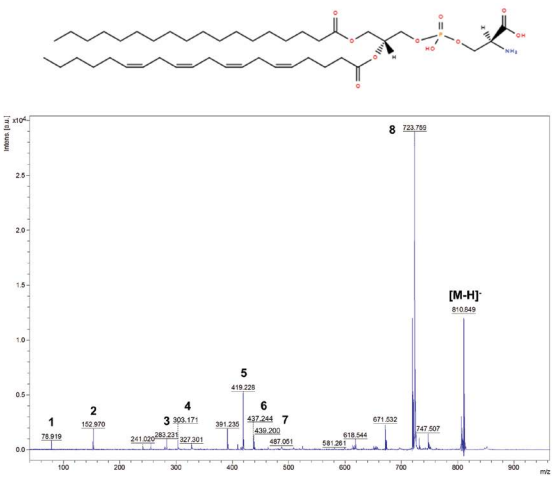

m/z	Description
[M-H]-	Precursor ion
8	Loss of serine from precursor ion
7	Neutral loss of sn1 RCOOH group and serine from [M-H]-
6	Loss of sn2 acyl chain as (RCH=C=O) and serine from [M-H]-
5	Neutral loss of sn2 RCOOH group and serine from [M-H]-
4	sn2 RCOO- ion
3	sn1 RCOO- ion
2	2,5-dihydroxybenzoic acid (matrix) Glycerol-3-phosphate ion with loss of H2O
1	PO3- ion

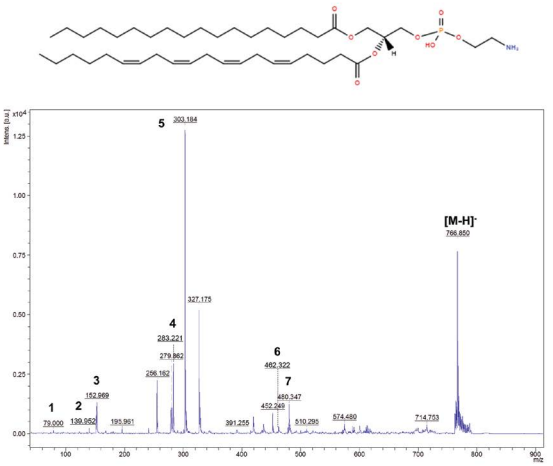

m/z	Description
[M-H]-	Precursor ion
7	Loss of sn2 acyl chain as (RCH=C=O) from [M-H]-
6	Neutral loss of sn2 RCOOH group from [M-H]-
5	sn2 RCOO- ion
4	sn1 RCOO- ion
3	2,5-dihydroxybenzoic acid (matrix) Glycerol-3-phosphate ion with loss of H2O
2	Ethanolamine phosphate ion
1	PO3- ion

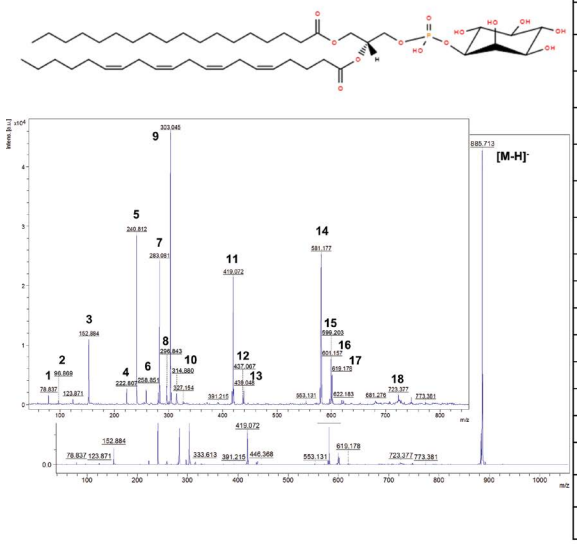

m/z	Description
[M-H]-	Precursor ion
18	Loss of inositol from [M-H]-
17	Loss of sn1 acyl chain as (RCH=C=O) from [M-H]-
16	Neutral loss of sn1 RCOOH group from [M-H]-
15	Loss of sn2 acyl chain as (RCH=C=O) from [M-H]-
14	Neutral loss of sn2 RCOOH group from [M-H]-
13	Neutral loss of sn1 RCOOH group and inositol from [M-H]-
12	Loss of sn2 acyl chain as (RCH=C=O) and inositol from [M-H]-
11	Neutral loss of sn2 RCOOH group and inositol from [M-H]-
10	Glycerophosphoinositol - H2O
9	sn2 RCOO- ion
8	Glycerophosphoinositol - 2H2O
7	sn1 RCOO- ion
6	Loss of CO2 from sn2 RCOO- ion (PUFA)
5	Inositol phosphate ion
4	Inositol phosphate ion - H2O
3	2,5-dihydroxybenzoic acid (matrix) Glycerol-3-phosphate ion with loss of H2O
2	H2PO4- ion
1	PO3- ion

Figure 1: MALDI LIFT-TOF/TOF identified lipid signals in the negative ion mode. Fragment ions were searched in the LIPID MAPS dataset and identified (A) phosphatidylserines based on an m/z 810.8 and a characteristic [M-H-serine]- fragment ion m/z peak of 723.8, (B) phosphatidylethanolamine am/z 766.8, and (C) phosphatidylinositols (C18:0/C20:5) with m/z 885.7, inositol phosphate ion (m/z 241 or m/z 223 with loss of water), and glycerophosphoinositol minus water had m/z's of 297 or 315.

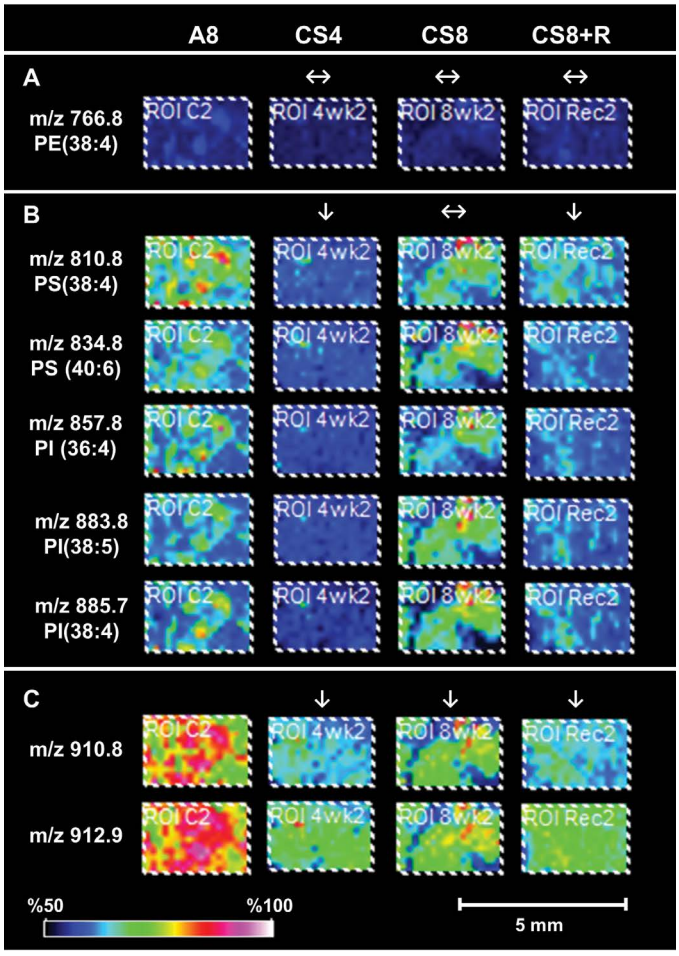

Figure 2: Representative MALDI-IMS results showing regional distributions and levels of 8 distinct m/z phosphatidylethanolamine (PE), phosphatidylserine (PS), or phosphatidylinositol (PI) species in livers from A/J adult mice exposed to air for 8 weeks (A8), cigarette smoke for 4 (CS4) or 8 (CS8) weeks, or CS8 followed by 2 weeks recovery on room air (CS8+R). Images were acquired in the negative ion mode. Lipid ion intensities are represented by the color scale and relative differences from control are indicated with directional arrows. Also see Table 1. Results are clustered into patterns reflecting relative effects of CS: A) no effect; B) phospholipids reduced most strikingly by CS4, unchanged or somewhat increased by CS8 and reduced to levels intermediate between those measured in CS4 and CS8 livers; and C) very high levels in A8 and similarly reduced by CS exposure, independent of duration and recovery.

most were reduced. Some responses were modulated by duration of CS exposure. The short period of recovery had three different effects, yielding similar or further shifted expression levels relative to CS8, or tended to reverse effects of CS exposures toward control.

Clustered lipid profiles based on CS durations and CS withdrawal

Principle component analysis (PCA) of the phospholipid ion profiles generated three distinct clusters: The A8 (control) cluster was separate from the three CS clusters, CS4 and CS8+R overlapped extensively but could be delineated with respect to sub-populations of lipid ions, and CS8 had its own dominant clustering with modest overlaps with CS8+R (Figure 5). Therefore, despite MALDI-IMS trends reflecting changes in various phospholipid ion intensities, the PCA revealed distinct effects of 4-week versus 8-week CS exposures and partial reversal of the CS8 effects by a short period of recovery (CS8+R).

Discussion

Tobacco smoke contains hundreds of volatile and non-volatile toxins, in addition to tobacco-specific nitrosamines. The two most abundant and potent tobacco-specific nitrosamines present in CS are 4-(methylnitrosamino)-1-(3-pyridyl)-1-butanone (NNK) and N'-nitrosonornicotine (NNN) [26,47,48]. In just one cigarette, tobacco-specific nitrosamine levels range from 1 μg and 9 μg, and other classes of nitrosamines can be as high as 8 μg of [49]. Furthermore, bystander, i.e., second-hand exposures can be up to 2 μg of nitrosamine products from burning tobacco. Until recently, most research on pathogenic effects of nitrosamines have centered on carcinogenesis; however, an emerging concept stemming from our research is that low-level nitrosamine exposures also threaten health by causing degenerative diseases linked to tissue injury, inflammation, impairments in insulin/IGF signaling through cell survival and metabolic pathways, oxidative and nitrosative stress, and dysregulated lipid metabolism [27,28,50-55]. Accordingly, we have shown that NNK and NDEA cause steatohepatitis, and can worsen liver injury caused by alcohol or chronic high dietary fat diet intake [27,52,53].

The present work drives at the main clinical and epidemiological concerns about the potential role of CS exposures as a mediator of chronic liver disease, and potential contributing factor in ALD pathogenesis. The research was focused on lipid biochemistry as a relatively novel method of characterizing metabolic liver diseases. We used MALDI-IMS to visualize, characterize and semi-quantify lipid

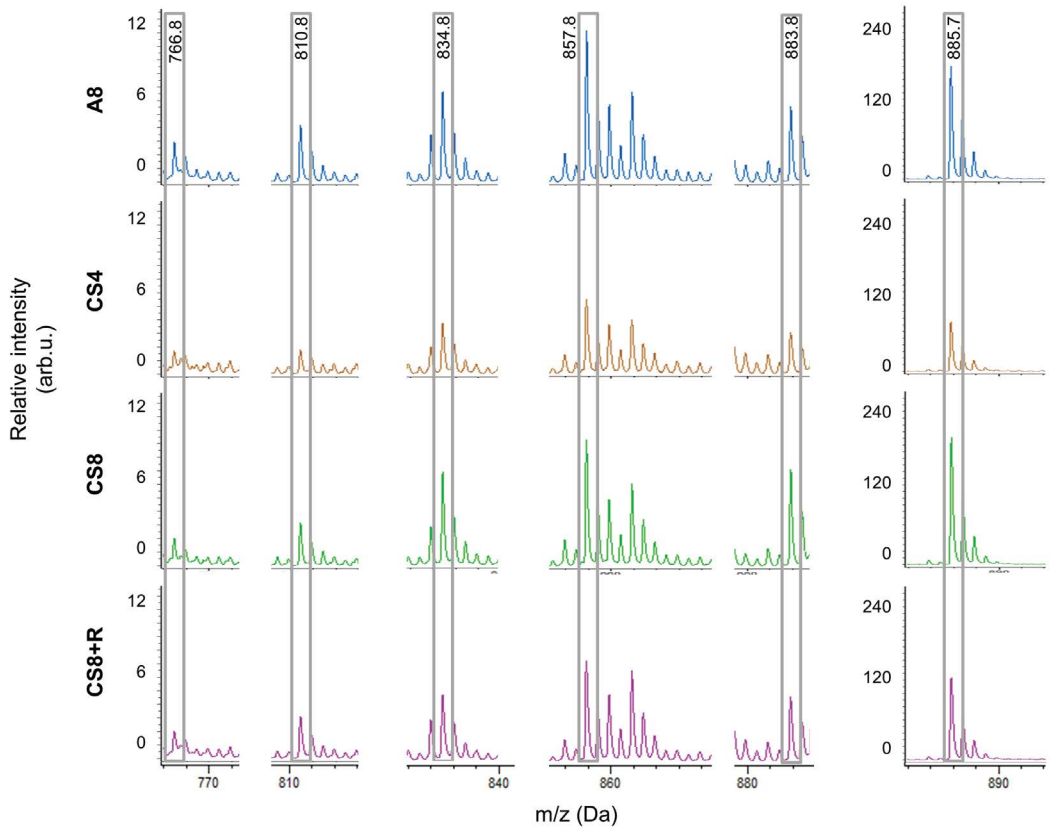

Figure 3: Relative intensity (abundance) of selected phospholipid species in livers from A8, CS4, CS8, and CS8+R A/J adult male mice. The boxes highlight the dominant peaks for 6 lipid ions. The vertical comparisons graphically display the findings by MALDI-IMS shown in Fig. 2. The relative intensities of the lipid ions detected from m/z 770 to 890 Da reveal prominent reductions in the CS4 group, relatively unchanged or slightly increased levels in the CS8 livers, and moderately reduced levels in livers from CS8+R mice. Note the change in scale needed for the m/z 890 profile compared with the one used for the other 5 phospholipid ions.

profile shifts that occurred following CS exposures and recovery. Data were analyzed using Clin-Pro Tools software, PCA, and R-generated heatmaps. With these approaches, responses to CS exposures and recovery were non-uniform. In selected groups of abundantly expressed lipid ions, we detected striking reductions in multiple phospholipids in the CS4 group, paradoxical partial normalization of responses in CS8 livers, but worsening of responses in the CS8+R group (Figures 2 and 3). However, from the PCA and heatmap figures (Figures 4 and 5), quite different responses were detected showing either similar or progressive (from CS4 to CS8) alterations in lipid ion expression, with similar or differential responses in the CS8+R group (see below). These findings suggest that while several aspects of hepatic lipid biochemistry may be adaptable/reversible from short- (4 weeks) to long-term (8 weeks) CS exposures, others changes persist or worsen, and are not consistently ameliorated by cessation of CS exposure. To some degree, the worsening of some hepatic lipid profiles that occurred after the recovery period could reflect withdrawal effects as can be seen with many drugs.

Phospholipids play critical roles in regulating cell membrane structural integrity, receptor functions, and microdomains (lipid rafts) [56-58]. Phosphatidylserines modulate cell cycle signaling by serving as cofactors that bind to signaling molecules, particularly those concerned with apoptosis [59]. Phosphatidylcholines are the most abundant phospholipids and critical to all cells. Phosphatidylcholine biosynthesis is regulated by methylation of phosphatidylethanolamine in the liver [59,60], and its degradation is mediated by Phopholipase D hydrolysis to phosphatidic acid and choline. Phosphatidylcholines have diverse functions as they: 1) circulate in peripheral blood as integral components of lipoproteins such as high density lipoprotein; 2) are precursors of sphingomyelin and regulate sphingomyelin metabolic pathways; 3) regulate signaling via plasmalogen and diacylglycerols; and 4) may have a functional role in liver repair. Phosphatidyinositides including stearic acid and arachidonic acid, have important roles in lipid signaling, membrane (vesicle) trafficking, and cellular signaling [61,62]. Phosphatidylethanolamines comprise nearly a quarter of all phospholipids in mammalian cells, and are even more abundantly expressed in central nervous system white matter where they comprise up to 45% of the phospholipids. Phosphatidylethanolamines regulate membrane curvature, increase membrane viscosity, and play important roles in lipoprotein secretion in liver [59,63].

Reduced phospholipid levels have been linked to insulin resistance, including in liver [64] and decreased phosphatidylinositol-3'-kinase [65] or increased phospholipase activity [66-69]. Therefore, CS-mediated reductions in hepatic phospholipid levels could impair insulin/IGF signaling as occurs with NNK exposure [27,28]. Of note is that tobacco-specific nitrosamines decrease lung phospholipids (phosphatidylcholine, phosphatidylglycerol, and phosphatidylserine) by enhancing phospholipase A2 activity [70]. Moreover, nitrosamine-induced reductions in phospholipids can be accompanied by increases in neutral lipids [71]. Therefore, tobacco-specific nitrosamines in CS may mediate their adverse effects on insulin/IGF signaling in liver by inhibiting phospholipid synthesis or maintenance via increased activation of Phospholipase B. Persistence or worsening of lipid ion profile shifts over time, despite CS withdrawal, suggests that CS-

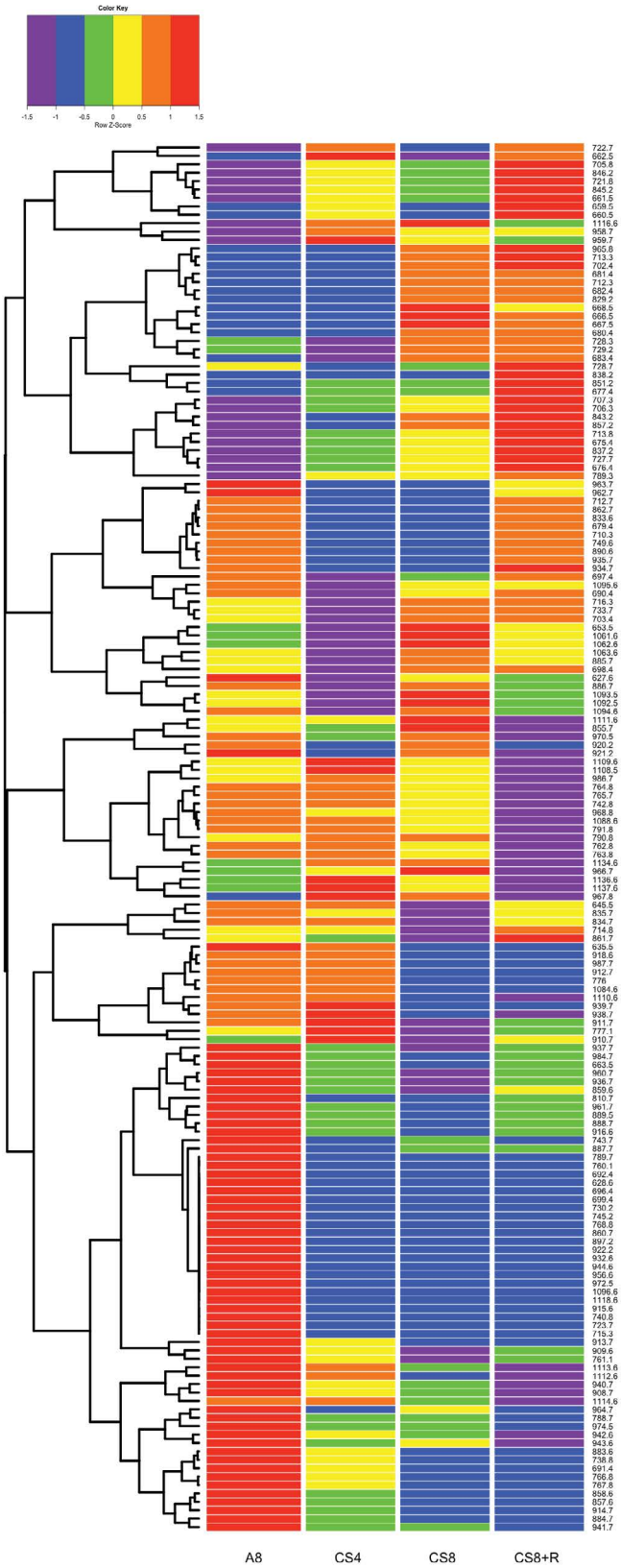

Figure 4: Heatmap illustrates hierarchical clustering of different lipid ion species. Results shown with the 6-color palette correspond to z-scores, which were scaled to have a mean of 0 and S.D. of 1. A hierarchical clustering algorithm was applied using the Euclidean distance function on the overall table to display a dendrogram of lipid ions. A8=control room air exposed x 8 wks; CS4=cigarette smoke exposed x 4 wks; CS8=cigarette smoke exposed x 8 wks; CS8+R=cigarette smoke exposed x 8 wks followed by 2 wks recovery in room air.

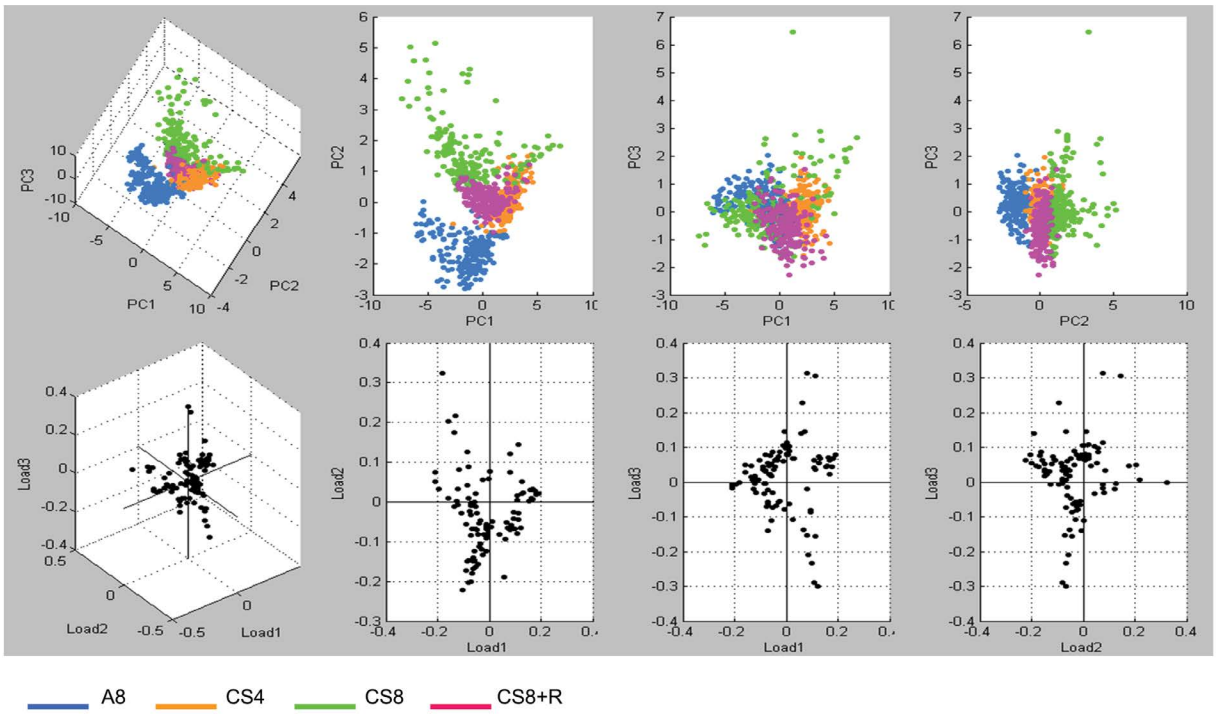

Figure 5: Principal component analysis (PCA) of IMS data acquired in the negative-ionization mode. PCA was performed using the total MS spectra generated from the ROI's in each group using ClinProTools. Based on spectral similarities and hepatic lipid profiles, three distinct groupings were identified: the A8 control and C8+R overlapped, while CS4 and CS8 formed distinct clusters.

mediated impairments in phospholipid homeostasis may become irreversible.

Hierarchical heatmap dendrograms and PCA were used to examine effects of CS exposures on the full range of lipid ions detected in liver. Those complementary analyses demonstrated greater variability in the responses to CS exposures, duration of exposure, and recovery compared with the more targeted studies detailed above. Importantly, the expression levels of large clusters of lipid ions were either increased or decreased with CS exposures, and the effects of longer exposures were either greater or similar to those observed with shorter exposures. This suggests that hepatic lipid ion responses to CS exposures can be all-or-none, i.e., sustained or progressive. The finding that short-term recovery tended to normalize expression of some lipid ions is encouraging, and consistent with the concept that metabolic abnormalities cause by CS exposure are to some degree reversible. However, since most of the adverse effects of CS were not resolved, and in several instances they were made worse after the period of recovery, a major concern is that many abnormalities caused by CS exposure may be permanent, difficult to reverse, or prone to progress over time, even in the absence of continued CS exposures.

Acknowledgements

Supported by AA-11431 and AA-12908 from the National Institutes of Health and the Tobacco-Related Disease Research Program Grant 17RT-0171.

References

1. Miller AM, Horiguchi N, Jeong WI, Radaeva S, Gao B (2011) Molecular mechanisms of alcoholic liver disease: innate immunity and cytokines. Alcohol Clin Exp Res 35: 787-793.
2. McCullough AJ, O'Shea RS, Dasarathy S (2011) Diagnosis and management of alcoholic liver disease. J Dig Dis 12: 257-262.
3. Paula H, Asrani SK, Boetticher NC, Pedersen R, Shah VH, et al. (2010) Alcoholic liver disease-related mortality in the United States: 1980-2003. Am J Gastroenterol 105: 1782-1787.
4. O'Shea RS, Dasarathy S, McCullough AJ (2010) Practice Guideline Committee of the American Association for the Study of Liver Diseases; Practice Parameters Committee of the American College of Gastroenterology, Alcoholic liver disease. Hepatology 51: 307-328.
5. Purohit V, Gao B, Song BJ (2009) Molecular mechanisms of alcoholic fatty liver. Alcohol Clin Exp Res 33: 191-205.
6. Vidali M, Stewart SF, Albano E (2008) Interplay between oxidative stress and immunity in the progression of alcohol-mediated liver injury. Trends Mol Med 14: 63-71.
7. de la Monte SM, Yeon JE, Tong M, Longato L, Chaudhry R, et al. (2008) Insulin resistance in experimental alcohol-induced liver disease. J Gastroenterol Hepatol e477-486.
8. Pang M, de la Monte SM, Longato L, Tong M, He J, et al. (2009) PPARdelta agonist attenuates alcohol-induced hepatic insulin resistance and improves liver injury and repair. J Hepatol 50: 1192-1201.
9. Ramirez T, Longato L, Dostalek M, Tong M, Wands JR, et al. (2013) Insulin resistance, ceramide accumulation, and endoplasmic reticulum stress in human chronic alcohol-related liver disease. Alcohol Alcohol 48: 39-52.
10. Cohen JI, Nagy LE (2011) Pathogenesis of alcoholic liver disease: interactions between parenchymal and non-parenchymal cells. J Dig Dis 12: 3-9.
11. Derdak Z, Lang CH, Villegas KA, Tong M, Mark NM, et al. (2011) Activation of p53 enhances apoptosis and insulin resistance in a rat model of alcoholic liver disease. J Hepatol 54: 164-172.
12. McVicker BL, Tuma DJ, Kubik JL, Tuma PL, Casey CA (2006) Ethanol-induced apoptosis in polarized hepatic cells possibly through regulation of the Fas pathway. Alcohol Clin Exp Res 30: 1906-1915.
13. de la Monte SM, Longato L, Tong M, DeNucci S, Wands JR (2009) The liver-brain axis of alcohol-mediated neurodegeneration: role of toxic lipids. Int J Environ Res Public Health 6: 2055-2075.
14. Ronis MJ, Butura A, Korourian S, Shankar K, Simpson P, et al. (2008) Cytokine and chemokine expression associated with steatohepatitis and hepatocyte proliferation in rats fed ethanol via total enteral nutrition. Exp Biol Med (Maywood) 233: 344-355.

15. Malhi H, Kaufman RJ (2011) Endoplasmic reticulum stress in liver disease. J Hepatol 54: 795-809.

16. Pandol SJ, Gorelick FS, Gerloff A, Lugea A (2010) Alcohol abuse, endoplasmic reticulum stress and pancreatitis. Dig Dis 28: 776-782.

17. Feldstein AE, Bailey SM (2011) Emerging role of redox dysregulation in alcoholic and nonalcoholic fatty liver disease. Antioxid Redox Signal 15: 421-424.

18. Kaplowitz N, Ji C (2006) Unfolding new mechanisms of alcoholic liver disease in the endoplasmic reticulum. J Gastroenterol Hepatol 21 Suppl 3: S7-9.

19. Ding WX, Manley S, Ni HM (2011) The emerging role of autophagy in alcoholic liver disease. Exp Biol Med (Maywood) 236: 546-556.

20. Banerjee K, Mohr L, Wands JR, de la Monte SM (1998) Ethanol inhibition of insulin signaling in hepatocellular carcinoma cells. Alcohol Clin Exp Res 22: 2093-2101.

21. Romberger DJ, Grant K (2004) Alcohol consumption and smoking status: the role of smoking cessation. Biomed Pharmacother 58: 77-83.

22. Kalman D, Kim S, DiGirolamo G, Smelson D, Ziedonis D (2010) Addressing tobacco use disorder in smokers in early remission from alcohol dependence: the case for integrating smoking cessation services in substance use disorder treatment programs. Clin Psychol Rev 30: 12-24.

23. Trushin N, Hecht SS (1999) Stereoselective metabolism of nicotine and tobacco-specific N-nitrosamines to 4-hydroxy-4-(3-pyridyl)butanoic acid in rats. Chem Res Toxicol 12: 164-171.

24. Hoffmann D, Hecht SS, Ornaf RM, Wynder EL (1974) N'-nitrosonornicotine in tobacco. Science 186: 265-267.

25. Hecht SS, Ornaf RM, Hoffmann D (1975) Chemical studies on tobacco smoke. XXXIII. N' -nitrosonornicotine in tobacco: analysis of possible contributing factors and biologic implications. J Natl Cancer Inst 54: 1237-1244.

26. Stepanov I, Feuer R, Jensen J, Hatsukami D, Hecht SS (2006) Mass spectrometric quantitation of nicotine, cotinine, and 4-(methylnitrosamino)-1-(3-pyridyl)-1-butanol in human toenails. Cancer Epidemiol Biomarkers Prev 15: 2378-2383.

27. Zabala V, Tong M, Yu R, Ramirez T, Yalcin EB, et al. (2015) Potential contributions of the tobacco nicotine-derived nitrosamine ketone (NNK) in the pathogenesis of steatohepatitis in a chronic plus binge rat model of alcoholic liver disease. Alcohol Alcohol 50: 118-131.

28. Yalcin EB, Nunez K, Cornett DS, de la Monte SM (2015) Differential Lipid Profiles in Experimental Steatohepatitis: Role for Imaging Mass Spectrometry as a Diagnostic Aid. Journal of Drug and Alcohol Research 4: 1-11.

29. Witschi H, Espiritu I, Suffia M, Pinkerton KE (2002) Expression of cyclin D1/2 in the lungs of strain A/J mice fed chemopreventive agents. Carcinogenesis 23: 289-294.

30. Gordon T, Bosland M (2009) Strain-dependent differences in susceptibility to lung cancer in inbred mice exposed to mainstream cigarette smoke. Cancer Lett 275: 213-220.

31. March TH, Wilder JA, Esparza DC, Cossey PY, Blair LF, et al. (2006) Modulators of cigarette smoke-induced pulmonary emphysema in A/J mice. Toxicol Sci 92: 545-559.

32. Agarwal AR, Yin F, Cadenas E (2014) Short-term cigarette smoke exposure leads to metabolic alterations in lung alveolar cells. Am J Respir Cell Mol Biol 51: 284-293.

33. Agarwal AR, Zhao L, Sancheti H, Sundar IK, Rahman I, et al. (2012) Short-term cigarette smoke exposure induces reversible changes in energy metabolism and cellular redox status independent of inflammatory responses in mouse lungs. Am J Physiol Lung Cell Mol Physiol 303: 889-898.

34. Groman E, Blauensteiner D, Kunze U, Schoberberger R (2000) Carbon monoxide in the expired air of smokers who smoke so-called "light" brands of cigarettes. Tob Control 9: 352.

35. Setshedi M, Longato L, Petersen DR, Ronis M, Chen WC, et al. (2011) Limited Therapeutic Effect of N-Acetylcysteine on Hepatic Insulin Resistance in an Experimental Model of Alcohol-Induced Steatohepatitis. Alcohol Clin Exp Res 35: 2139-2151.

36. Angel PM, Spraggins JM, Baldwin HS, Caprioli R (2012) Enhanced sensitivity for high spatial resolution lipid analysis by negative ion mode matrix assisted laser desorption ionization imaging mass spectrometry. Anal Chem 84: 1557-1564.

37. Pavia DL, Lampman GM, Kriz GSJ (1982) Introduction to Organic Laboratory Techniques: A Contemporary Approach, New York: Saunders College Publishing.

38. Hankin JA, Barkley RM, Murphy RC (2007) Sublimation as a method of matrix application for mass spectrometric imaging. J Am Soc Mass Spectrom 18: 1646-1652.

39. Bergkvist A, Rusnakova V, Sindelka R, Garda JM, Sjögreen B, et al. (2010) Gene expression profiling--Clusters of possibilities. Methods 50: 323-335.

40. Dean CB, Nielsen JD (2007) Generalized linear mixed models: a review and some extensions. Lifetime Data Anal 13: 497-512.

41. Walch A, Rauser S, Deininger SO, Höfler H (2008) MALDI imaging mass spectrometry for direct tissue analysis: a new frontier for molecular histology. Histochem Cell Biol 130: 421-434.

42. Cornett DS, Reyzer ML, Chaurand P, Caprioli RM (2007) MALDI imaging mass spectrometry: molecular snapshots of biochemical systems. Nat Methods 4: 828-833.

43. Gessel MM, Norris JL, Caprioli RM (2014) MALDI imaging mass spectrometry: spatial molecular analysis to enable a new age of discovery. J Proteomics 107: 71-82.

44. Caprioli RM, Farmer TB, Gile J (1997) Molecular imaging of biological samples: localization of peptides and proteins using MALDI-TOF MS. Anal Chem 69: 4751-4760.

45. Fahy E, Subramaniam S, Murphy RC, Nishijima M, Raetz CR, et al. (2009) Update of the LIPID MAPS comprehensive classification system for lipids. J Lipid Res 50 Suppl: S9-14.

46. Shevchenko A, Simons K (2010) Lipidomics: coming to grips with lipid diversity. Nat Rev Mol Cell Biol 11: 593-598.

47. Stepanov I, Hecht SS (2005) Tobacco-specific nitrosamines and their pyridine-N-glucuronides in the urine of smokers and smokeless tobacco users. Cancer Epidemiol Biomarkers Prev 14: 885-891.

48. Stepanov I, Hecht SS (2008) Detection and quantitation of N'-nitrosonornicotine in human toenails by liquid chromatography-electrospray ionization-tandem mass spectrometry. Cancer Epidemiol Biomarkers Prev 17: 945-948.

49. Tricker AR, Ditrich C, Preussmann R (1991) N-nitroso compounds in cigarette tobacco and their occurrence in mainstream tobacco smoke. Carcinogenesis 12: 257-261.

50. de la Monte SM, Tong M (2009) Mechanisms of nitrosamine-mediated neurodegeneration: potential relevance to sporadic Alzheimer's disease. J Alzheimers Dis 17: 817-825.

51. de la Monte SM, Tong M, Lawton M, Longato L (2009) Nitrosamine exposure exacerbates high fat diet-mediated type 2 diabetes mellitus, non-alcoholic steatohepatitis, and neurodegeneration with cognitive impairment. Mol Neurodegener 4: 54.

52. Tong M, Neusner A, Longato L, Lawton M, Wands JR, et al. (2009) Nitrosamine exposure causes insulin resistance diseases: relevance to type 2 diabetes mellitus, non-alcoholic steatohepatitis, and Alzheimer's disease. J Alzheimers Dis 17: 827-844.

53. Andreani T, Tong M, de la Monte SM (2014) Hotdogs and Beer: Dietary Nitrosamine Exposure Exacerbates Neurodevelopmental Effects of Ethanol in Fetal Alcohol Spectrum Disorder. Journal of Drug and Alcohol Research 3: 1-9.

54. Tong M, Yu R, Deochand C, de la Monte SM (2015) Differential Contributions of Alcohol and the Nicotine-Derived Nitrosamine Ketone (NNK) to Insulin and Insulin-Like Growth Factor Resistance in the Adolescent Rat Brain. Alcohol Alcohol 50: 670-679.

55. Yalcin EB, Nunez K, Tong M, de la Monte SM (2015) Differential Sphingolipid and Phospholipid Profiles in Alcohol and Nicotine-Derived Nitrosamine Ketone-Associated White Matter Degeneration. Alcohol Clin Exp Res 39: 2324-2333.

56. Mollinedo F, Gajate C (2015) Lipid rafts as major platforms for signaling regulation in cancer. Adv Biol Regul 57: 130-146.

57. Ma DW (2007) Lipid mediators in membrane rafts are important determinants of human health and disease. Appl Physiol Nutr Metab 32: 341-350.

58. Vainio S, Bykov I, Hermansson M, Jokitalo E, Somerharju P, et al. (2005) Defective insulin receptor activation and altered lipid rafts in Niemann-Pick type C disease hepatocytes. Biochem J 391: 465-472.

59. Vance DE (2013) Physiological roles of phosphatidylethanolamine N-methyltransferase. Biochim Biophys Acta 1831: 626-632.

60. Vance DE (2014) Phospholipid methylation in mammals: from biochemistry to physiological function. Biochim Biophys Acta 1838: 1477-1487.

61. Phillips SE, Vincent P, Rizzieri KE, Schaaf G, Bankaitis VA, et al. (2006) The diverse biological functions of phosphatidylinositol transfer proteins in eukaryotes. Crit Rev Biochem Mol Biol 41: 21-49.

62. Tilley SJ, Skippen A, Murray-Rust J, Swigart PM, Stewart A, et al. (2004) Structure-function analysis of human phosphatidylinositol transfer protein alpha bound to phosphatidylinositol. Structure 12: 317-326.

63. Vance JE, Tasseva G (2013) Formation and function of phosphatidylserine and phosphatidylethanolamine in mammalian cells. Biochim Biophys Acta 1831: 543-554.

64. Payne F, Lim K, Girousse A, Brown RJ, Kory N, et al. (2014) Mutations disrupting the Kennedy phosphatidylcholine pathway in humans with congenital lipodystrophy and fatty liver disease. Proc Natl Acad Sci U S A 111: 8901-8906.

65. Müller G, Frick W (1999) Signalling via caveolin: involvement in the cross-talk between phosphoinositolglycans and insulin. Cell Mol Life Sci 56: 945-970.

66. Müller G, Schulz A, Wied S, Frick W (2005) Regulation of lipid raft proteins by glimepiride- and insulin-induced glycosylphosphatidylinositol-specific phospholipase C in rat adipocytes. Biochem Pharmacol 69: 761-780.

67. Jacobs C, Onnockx S, Vandenbroere I, Pirson I (2004) Endogenous SHIP2 does not localize in lipid rafts in 3T3-L1 adipocytes. FEBS Lett 565: 70-74.

68. Tilg H, Moschen A (2010) Update on nonalcoholic fatty liver disease: genes involved in nonalcoholic fatty liver disease and associated inflammation. Curr Opin Clin Nutr Metab Care 13: 391-396.

69. Shashkin PN, Wasner HK, Ortmeyer HK, Hansen BC (2001) Prostaglandylinositol cyclic phosphate (cPIP): a novel second messenger of insulin action. Comparative analysis of two kinds of “insulin mediators”. Diabetes Metab Res Rev 17: 273-284.

70. Vijayaraj P, Sivaprakasam C, Varthini LV, Sarkar M, Nachiappan V (2014) In vitro exposure of tobacco specific nitrosamines decreases the rat lung phospholipids by enhanced phospholipase A2 activity. Toxicol In Vitro 28: 1097-1105.

71. Vijayaraj P, Sabarirajan J, Nachiappan V (2011) Enhanced phospholipase B activity and alteration of phospholipids and neutral lipids in Saccharomyces cerevisiae exposed to N-nitrosonornicotine. Antonie Van Leeuwenhoek 99: 567-577.